

Response to reviews & editorial comments: King et al., Geochronology

Interactive comment on “ESR-thermochronometry of the Hida range of the Japanese Alps: Validation and future potential” by Georgina E. King et al.

Nathan Brown (Referee) nathan.brown@berkeley.edu

This study is a thorough and compelling application of ESR to low-temperature thermochronology to the Japanese Alps. The authors have put forward a tremendous effort to present a detailed comparison of multi-elevated-temperature IRSL results from feldspar against Al and Ti ESR centers within quartz. The results are encouraging and provide the reader with a broad overview of why such an advance is worthwhile (similar stability to OSL signals but applicable for slower cooling rates), while still carefully outlining methodology limitations (e.g., lack of automated measurement capabilities and uncertainties associated with reaction kinetics). Below, I offer several questions I had while reading along with a few suggestions or concerns.

Main text:

p.2,l.20: The averaging time(s) would be helpful for these rates.

Unfortunately this information is not given in the original publication, so it is not possible to add it to the text. As the saturation limits of the sample are also not described in the original paper, it is not possible for us to calculate the validity of these cooling rates for a particular time period.

p.2,l.30: Slightly unclear what 'paired' means in this context.

Removed paired.

p.3,l.4: Here you could also mention that signal intensity is a persistent limitation for quartz OSL thermochronometry (unlike for ESR, apparently).

As we have only explored this sample set at this point in time, we are reluctant to make a general statement about the behaviour of quartz ESR-thermochron signals. For this reason we respectfully choose not to make this addition.

p.3,Eq.10ff.: The negative sign before the activation energy is difficult to see with the current typesetting.

We have added an additional space which makes the negative sign clearer.

p.3,l.30: "...a model that assumes a Gaussian distribution of activation energies, E_a around the mean trap depth, $\mu(E_t)$ (eV)." It would be good to also mention the meaning of $\sigma(E_t)$ here. Besides the Lambert study in review, is there any precedent in ESR literature for treating the activation energy in this way? The reason for adopting this approach probably deserves either an available citation or further justification in the main text, even if only a sentence or two. The full explanation within the Supplementary Materials is excellent, but a quick note here would be good.

We believe that it is the first time that ESR signals have been modelled in this way. We added the following to the main text:

An alternative approach could be to use a first or second order kinetic model as has been done previously (Toyoda and Ikeya, 1991; Ikeya, 1993; Grün et al., 1999) and we discuss our model selection more completely in the supplementary material.

p.4,II.8-9: Is this owing to the long irradiation times with common beta sources?

Because of the comparatively large volume of sample measured in ESR dating, it is not possible to use a beta source for irradiation. Multiple aliquot methods relate to the physical distance between gamma sources and measurement facilities, which mean that it is more convenient to dose multiple aliquots prior to measurement which must be done elsewhere. We have amended the sentence to make this clearer:

The former approach has only recently been made practical, following the introduction of X-ray irradiation for regenerative dosing (Oppermann and Tsukamoto, 2015), as opposed to gamma irradiation which is often done at a laboratory separate to the measurement laboratory.

p.5,I.23: It seems misleading to label alpha as a 'constant' when it has a known functional form (e.g., Chen and McKeever, 1997, pp. 60-66) that depends upon the trap depth (which is often allowed to vary in studies such as this).

Amended to "alpha is a constant related to the Bohr radius of the electron trap".

p.5,I.27: I believe that 'charge' encompasses electrons and electron holes.

Agreed and amended.

p.6,II.20-22: It seems important to qualify here that this result hinges on the assumption of a correct kinetic expression; this statement should not be misunderstood to mean that the authors have (at this stage in the manuscript) successfully recovered age information from slowly cooling samples, but that, to the degree that the kinetic expressions are accurate, slow cooling histories should be within resolution.

We think that this is implicit in the exercise performed here as it also holds for the OSL data described in the preceding lines, and prefer not to make any further qualification.

p.9,I.22: Strictly, you have quantified the room temperature detrapping. Presumably there is little thermal detrapping involved, but might be worth mentioning briefly to avoid confusion with LNT fading measurements.

We have inserted "at room temperature" to be explicit that these measurements were not made at LNT.

p.11,I.19: That IRSL_50 signals are saturated and higher temperature signals are unsaturated in the same sample seems to me an inexplicable result. Can you comment on why this might be observed?

This is not an uncommon observation for thermochronometry data (although much of these data remain unpublished at this time). It is simply because the IRSL50 signals exhibit much greater rates of fading than the higher temperature signals, meaning that they reach athermal steady state more rapidly. We have added this sentence for clarification:

“Saturation of the IRSL₅₀ signals relative to the higher temperature signals is a consequence of their relatively high rate of anomalous fading”

p.11,l.24: I could not find the King et al. (2018) citation within the references. 'Athermal field saturation values' seems to be an inappropriate concept. Even for traps which are considered stable over burial timescales (e.g., qz fast component), we still discuss 'trap lifetimes.' The same practice should apply for thermal detrapping that happens within feldspars at Earth's surface. Field saturation should therefore be understood to reflect athermal and thermal loss processes, even if athermal loss is expected to be dominant at lower temperatures.

We follow the nomenclature of Kars et al. (2008); Valla et al. (2016) – QG and King et al. (2016) – QG. It is not necessary to invoke any thermal loss to explain the trapped charge concentrations of these samples, hence we refer to the athermal field saturation values. These values were calculated assuming no thermal losses using equation 8 in King et al. (2016) which is equivalent to equation 15 of Li and Li (2008). If we recalculated the trapped-charge concentrations using the full differential equation, i.e. including both thermal and athermal losses, the values would not change significantly, reflecting low rates of thermal detrapping at the surface temperatures experienced in this region. We prefer not to amend the text which clearly states that these values are calculated on an athermal basis. The citation to King et al. (2018) has now been included in the references.

p.11,l.32: Given that samples were taken from a transect that spans 1.2 km of elevation gain, shouldn't we expect more (and systematic) temperature variation with elevation? Most adiabatic lapse rates result in temperature loss of just under 10C per km of gained elevation.

This is an interesting point that we have considered carefully. We were unable to find an average adiabatic lapse rate for the Japanese Alps in the literature, however as the climate here is humid, it is likely that the adiabatic lapse rate is closer to 5°C per km, rather than 10°C per km. As such, we think that our allowed uncertainty of ±5°C on our final temperature for the inversion is appropriate.

p.12,II.27-30: Is such variation in thermal stability between ESR and IRSL populations expected from previous work? Also, is there a reason to use OSL and IRSL interchangeably? I find it a little confusing and would prefer simply referring to 'luminescence' signals or IRSL results.

We are unaware of previous work that has compared the ESR and luminescence signal stability of the same samples. This is something that we plan to pursue in future research. We found it encouraging that using the relative age differences between the luminescence and ESR signals, we could then predict what the relative difference in thermal stability should be, and that our experimental data was consistent with these predictions.

We follow Guralnik et al. (2015) – EPSL in using OSL to refer to generic optically stimulated luminescence signals, rather than being more specific regarding the type of stimulation (i.e. infrared stimulation).

p.13,l.6: Please also mention that Grun et al. (1999) extracted quartz from granite.

Amended.

Supplementary Materials: From a physical standpoint, I'm a little dubious about the prediction that GOK decay predicts dose-dependent decay in a non-saturating system. The formulation of second order kinetics (Garlick and Gibson, 1948) was developed for a phosphor where retrapping was predicted to increase dramatically as traps filled, therefore slowing

recombination in a way that increases with dose. If, however, there is no upper limit to available trapping sites, this limitation should disappear. Therefore, I am skeptical that the transition from Eq.S3 to Eq.S7, while mathematically sound, is physically sensible.

This is a good point but for completeness we feel that is important to include this equation and consideration in the supplementary materials.

p.5,II.4-8: Wow! This difference in stability between OSL and ESR centers between samples is a really intriguing result!

p.5,I.17: "For all samples, the BTS model predicts..." Are there not many kinetic assumptions built into this prediction, including the nature and shape of the band-tail? In other words, could a higher stability be predicted if the tail were assumed to be quadratic or if the tailing factor were higher? Or, are all of these values sufficiently quantified for these samples? Perhaps this is what you reference in the final sentences of this paragraph?

Here when we refer to BTS or GAU a certain distribution of band-tails is implicit. I.e. for the BTS we assume an exponential distribution of band-tails below the conduction band, whereas for GAU we instead assume a distribution of activation energies around the trap depth. The absolute value of the distribution (i.e. band-tail width, or width of the Gauss distribution around the trap depth) is determined from fitting the isothermal holding data for that particular sample and system. The GAU model predicts higher thermal stability than the BTS model, because it assumes a different energy distribution.

We have added "sample-specific" to make it clearer that these values are calculated for the particular sample under investigation. The distributions assumed for the GAU and BTS models are described in equations 4 and 7 respectively.

Anonymous Referee #2

This is the first paper reporting the thermochronology with both luminescence and ESR dating techniques. I strongly recommend this paper to be published after clarifying the points below.

(1) Last part of Chapter 3 and latter half of Fig.1: The authors once calculated the change with time of each signal intensity (Figs. 1b and c), then, using these results, they inverted to obtain the predicted cooling histories. Therefore, ideally, the red lines in latter half of Fig. 1 matches the white dashed lines, if I understand correctly. However, some of them are not. The authors should explain and discuss this point more clearly. It would partly because of the assumed initial condition, but there are cases that cannot be accepted, especially, slowest cooling rates for OSL centers. Probably, the discussion should be as such, in a case that the predicted cooling history obtained from OSL centers does not match that of ESR centers, the latter should be adopted. Then, this shall be applied to actual cases, i.e., Fig. 4.

Thank you for raising this important point. The reviewer is correct that the exercise shown in Fig. 1 tests whether the prescribed white line cooling histories can be recovered by inverting the forward modelled data shown in Figs 1a-c. The mis-match between the red and white lines provides some indication of signal performance, however the red-line is the median model of the accepted cooling histories used to generate the probability density function shown and rather the comparison should be made relative to the white line and brightly shaded parts of the PDFs. We have amended the latter part of section 3.2 to make this clearer by adding two sentences:

The results of the forward modelling and the synthetic inversions for the ESR and OSL data are shown in Fig. 1. The OSL signals for all cooling histories reach saturation (Fig. 1c), and this is reflected in the failure of the OSL to recover any of the cooling histories when inverted. This is

apparent because the 1σ confidence intervals show a broad range, with the highest density of cooling histories concentrated at temperatures $< 20\text{ }^{\circ}\text{C}$ over the past 500 ka indicating that the luminescence signals are saturated (as shown in Fig. 1c). The minimum cooling rate that can be resolved using OSL for sample KRG16-06 is $\sim 160\text{ }^{\circ}\text{C}/\text{Myr}$, calculated from 86% of the luminescence signal saturation level. Signal saturation is the key limitation that restricts the application of luminescence thermochronometry to regions undergoing rapid exhumation. In contrast, it is clear that the ESR data are able to resolve the $100\text{ }^{\circ}\text{C}/\text{Myr}$, $75\text{ }^{\circ}\text{C}/\text{Myr}$ and $50\text{ }^{\circ}\text{C}/\text{Myr}$ synthetic cooling histories, and cooling rates of $25\text{ }^{\circ}\text{C}/\text{Myr}$ are distinct from isothermal holding at $0\text{ }^{\circ}\text{C}$ over timescales of $\sim 2\text{ Ma}$. This is apparent because of the coincidence between the prescribed cooling histories (white lines) and the highest density of accepted cooling histories shown by the brightest colours in the probability density functions. These results are significant as they show that ESR-thermochronometry is applicable in a range of geological settings beyond the rapidly exhuming locations that luminescence-thermochronometry is currently restricted to.

(2) Discussions for Fig. 4: Probably, for samples KRG16-101 and 104, the results for all signals seems consistent, however, for the other two samples, they look inconsistent. The authors may use the criterion in (1), or may abandon the modelling. There should be cases that the results from different signals are not consistent with each other, then modelling of cooling history cannot be made from the statistical point of view. Probably Eq 10 would be for this. What are the L values for these?

The reviewer is correct that it is easier to combine some ESR/OSL signals than others. The reason is likely a combination of factors including natural sample variability, experimental data and/or numerical model limitations. In order to treat the data objectively, all numerical modelling was done under the same conditions i.e. with the same initial condition, over the same time-period with the same range of final temperatures and for the same number of iterations. As it was comparatively challenging to fit KRG16-06 fewer cooling histories were accepted after the values of L (Eqs. 9 and 10) were treated with the rejection algorithm i.e. L is contrasted with a random number between 0 and 1, if L is greater the cooling history is retained. The benefit of using this approach is that the full range of possible cooling histories are accepted. If the data could not be fitted, no cooling histories would be accepted, and this is something that we have observed multiple times for OSL data, but not for the samples presented here.

Detailed points

Page 2 line 6: "later" should be "at higher doses"

Amended.

Page 3 Eqs.1 and 2: " $E_a - \mu(E_t)$ " should be " E_a ".

Thank you for spotting this. We have amended the equation.

Page 5 eq. 5: The first term, " E_a " should be " E_b ", second term, " $E_t - E_b$ " should be " E_b ".

Thank you for spotting this. E_a should be E_b . Amended. However $E_t - E_b$ should not be E_b . E_b is the energy of the particular band-tail state, the total energy to escape the trap is $E_t - E_b$ i.e. the trap-depth minus the energy of the band-tail width.

Page 6 line 1: What is n_{mod} ?

We have clarified the sentence so that it reads:

“For each t-T path we calculated a misfit between the final inverted trapped-charge population, \tilde{n}_{mod} , and our forward modelled values, \tilde{n}_{fwd} (Wheelock et al., 2015),”

Thus n_{mod} is the final inverted trapped-charge population.

Page 6 lines 1-8: What is m? Probably number of traps.

Yes, this is defined on line 6 of the original submission “for m traps”.

Page 6 Eq. 9: Is this summation from 1 to m? If so, it is not clear.

This is summed over m traps. We do not know how to make the nomenclature clearer.

Page 7 line 17: Correct the inequality sign.

Sorry, however we are unsure what the reviewer is referring to. The quartz extracts have a density >2.58 and <2.70 hence $2.58 > \rho < 2.70 \text{ g cm}^{-3}$.

Page 8 line 7: “fitted” is by the least square method? How Ti-Li and Ti-H centers ratio was assumed?

Our measurements were carried out at $-150 \text{ }^\circ\text{C}$ which meant that we were unable to differentiate between the Ti-Li and Ti-H centres. We have added a sentence stating this explicitly to the text.

“As our measurements were carried out at $-150 \text{ }^\circ\text{C}$, it was not possible to differentiate between the Ti-H and Ti-Li centres, and consequently they have been treated as a single centre.”

Page 10 line 3: What is “signal intensity experiment”?

The signal intensity experiment is described in section 4.3.1 (page 9, line 14 of the original submission). It comprised measurement of how the signal intensity changed as a function of changing preheat treatment.

Page 10 line 3: Is “plateau” preheat plateau?

Yes, although not in the usual sense. It is a plateau in signal intensity with changing preheat temperature. We feel this is clear from the sentence “The signal intensity experiment indicates a plateau for the Ti-centre of sample KRG16-104 up until $160 \text{ }^\circ\text{C}$ ”

Section 5.1: One example of observed ESR spectrum should be shown together with a fitted spectrum.

We have added a new figure 2 showing an ESR spectrum for sample KRG16-06 and how the Al and Ti-centres were fitted.

Page 10 line 17: Correct the values and/or sample number.

Thank you for spotting this. Text updated.

Page 10 line 19: KRG16-112 is not listed in the Table.

No. This sample was used only in the dose recovery test. Therefore, it is not possible to include its details in this table. We amended the text on page 10, line 19 of the original submission to read "full dose response and isothermal decay was not measured for sample KRG16-112 and it is not included in Table 1"

Page 10 lines 20-23: Section 4.3.1 probably says the authors adopted regenerative protocol, but the dose response in Figs. 3 are additive dose.

The reviewer is correct and we tried to be explicit about this in the text. We measured the D_e values of our samples using a regenerative protocol as detailed in section 4.3.1. However, for measurement of the dose response into saturation we used an additive dose protocol. We have clarified this in the final sentence of section 4.3.2:

"Using a new aliquot of each sample, dose response was measured using the same measurement protocol, but omitting the zero-point measurement step, i.e. in an additive dose response protocol."

Page 13 line 1, Fig. 5: The signals seem to reduce too much. Please check the number in horizontal axis.

We re-checked these calculations and the figures are correct. Both the band-tail states model for luminescence and the GAUSS model used here for the ESR samples predict lower thermal stability than a single first order kinetic model.

Page 13 line 26, "consistent": Please describe how consistent

Qualifying how consistent the data are is difficult within the remit of this study, and is the focus of currently ongoing work. Ito et al. (2013; 2017) and Spencer et al. (2019) reported extremely young U-Pb and Zircon (U-Th-He) ages for this site. The fact that the luminescence data are not saturated is consistent with this. We have tried to give further information, whilst avoiding a lengthy discussion on this topic, which we feel is outside of the remit of this study, by amending this sentence to:

"The data inversions reveal that rates of rock cooling in the Hida range of the Japanese Alps are consistent with previous investigations that indicate rapid rock cooling (Ito et al., 2013; 2017; Spencer et al., 2019)."

Associate Editor comments

The authors' response to the reviewers' comments were mostly satisfactory and helped clarify the discussion. The one exception is one reviewer's complaint about the use of OSL as a generic name for all photon-induced luminescence. The authors' defended such use based on past practice. There may be past practice but I think it is a bad idea, and such practice should not be propagated. I was confused by the authors talking about OSL when they meant IRSL. I think the authors should use "luminescence" as a generic term, and use OSL meaning inducement by visible light and IRSL meaning inducement by infrared light.

We tested changing OSL to luminescence, but think that this will cause confusion. Revising OSL to luminescence makes the description of the analytical method even more vague (optical or thermal stimulation?) and further makes the reference to previous work which has been titled as OSL-thermochronometry (Guralnik et al., 2015-EPSL; King et al., 2016-QG; 2016-

Science; Herman and King, 2018-Elements) more challenging. If we refer to multi-IRSL-thermochronometry then it sounds like a new approach, which it is not. Equally, if we state IRSL, rather than OSL, it implies IRSL₅₀ rather than post-IR IRSL, or a MET protocol. For these reasons we remain of the opinion that OSL is a more appropriate term within the current manuscript.

Thermochronometry is a fairly specialized branch of trapped-charge dating, and I think the authors should not assume all their readers are such specialists. I think, in particular, they should describe briefly in non-mathematical terms the distinction between forward modeling and inverse modeling. I believe the former refers to modeling based on kinetic parameters and the latter to modeling based on dose response curves, but I am not sure. Explaining that will go along ways toward making the paper more accessible to non-specialists.

Thank you for this important comment. We have modified section 3 to provide this clarification:

“It is thus necessary to verify that ESR-thermochronometry offers advantages over luminescence methods. To achieve this, a series of synthetic tests for known cooling histories were done using the kinetic parameters of sample KRG16-06 (Table 1). These tests first comprised running a forward model, which uses sample-specific kinetic parameters and a rate equation to describe signal growth. Through forward modelling, it is possible to predict the trapped-charge concentration for a particular cooling history. The second stage of the test comprised inverting the trapped-charge concentrations predicted by the forward model, using the same rate equation, to determine if it is possible to recover the cooling history used in the forward model prediction. Further details of the forward and inverse modelling are given below.”

I found the discussion on intensity preheat plateau and equivalent dose preheat plateau somewhat opaque. One of the reviewers was also confused by this. The authors should explain better the purpose of the intensity plateau test.

I have included a citation to Murray and Wintle (2000) (Pg. 8, line 29) as essentially the preheat plateau is for the same purpose as in luminescence dating. I hope that this improves its clarity.

I have also added this sentence:

“On the basis of these experiments a preheat temperature of 160 °C was selected as this temperature maximises signal intensity (Fig. 3a) whilst remaining within the D_e value plateau (Fig. 3b).” (Pg. 10, line 22)

ESR-thermochronometry of the Hida range of the Japanese Alps: Validation and future potential

Georgina E. King¹, Sumiko Tsukamoto², Frédéric Herman¹, Rabiul H. Biswas¹, Shigeru Sueoka³ and Takahiro Tagami⁴

¹Institute of Earth Surface Dynamics, University of Lausanne, Lausanne, Switzerland

²Leibniz Institute for Applied Geophysics, Hannover, Germany

³Tono Geoscience Center, Japan Atomic Energy Agency, Toki, Japan

⁴Division of Earth and Planetary Sciences, Kyoto University, Kyoto, Japan

10 *Correspondence to:* Georgina E. King (georgina.king@unil.ch)

Abstract. The electron spin resonance (ESR) of quartz has previously been shown to have potential for determining rock cooling histories, however this technique remains underdeveloped. In this study, we explore the ESR of a suite of samples from the Hida range of the Japanese Alps. We develop measurement protocols and models to constrain the natural trapped charge concentration as well as the parameters that govern signal growth and signal thermal decay. The thermal stability of the Al and Ti-centres is similar to that of the luminescence of feldspar. Inverting the ESR data for cooling yields similar thermal histories to paired luminescence data from the same samples. However, a series of synthetic inversions show that whereas the luminescence of feldspar can only resolve minimum cooling histories of ~ 160 °C/Myr over timescales of 10^{3-5} a, quartz ESR may resolve cooling histories as low as 25-50 °C/Myr over timescales of 10^{3-7} a. This difference arises because quartz ESR has a higher dating limit than the luminescence of feldspar. These results imply that quartz ESR will be widely applicable in the constraint of late-stage rock cooling histories, providing new insights into landscape evolution over late-Quaternary timescales.

1. Introduction

Thermochronometry based on trapped-charge dating allows the constraint of late stage exhumation and/or rock thermal histories at the scale of glacial-interglacial cycles (e.g. Biswas et al., 2018). Following the study of Herman et al. (2010) which applied optically stimulated luminescence (OSL) dating to constrain the exhumation histories of the Southern Alps of New Zealand, there have been a number of both methodological and applied studies that have almost exclusively focused on luminescence dating (see King et al., 2016a and Herman and King, 2018 for reviews). In this study we explore the potential of a second trapped-charge dating method, electron spin resonance (ESR) of quartz, for ultra-low temperature (i.e. $< 100^\circ\text{C}$) thermochronometry.

Electron spin resonance can be used to measure the time-dependent accumulation of unpaired electrons (paramagnetic centres) in minerals such as quartz (cf. Grün, 1989; Ikeya, 1993). As for luminescence dating, when a mineral is exposed to ionizing radiation, electrons are excited from their ground state in the valence band, to the conduction band. Almost immediately most electrons fall back to the valence band, recombining with the “holes” of positive charge created by the electron’s excitation.

However, some electrons become trapped within defects in the crystal lattice, caused by element vacancies or substitutions. In this study we specifically target the Al (hole trapping) centre and the Ti (electron trapping) centre, although other defects such as the E' (oxygen vacancy) centre could also be investigated (e.g. Grün et al., 1999). The Al-centre comprises a hole located at AlO[•] (Nuttall and Weil, 1981) whereas the Ti-centre comprises the substitution of Si⁴⁺ with Ti³⁺+ e⁻ stabilized with H⁺, Li⁺ or Na⁺ (Rinneberg and Weil, 1972; Isoya et al., 1983). ESR offers a key advantage over luminescence dating, specifically that ESR signals saturate ~~later at~~ **higher doses** (Rink, 1997; Tsukamoto et al., 2018). Within the context of thermochronometry, this means that whilst the application of luminescence thermochronometry remains geographically limited to regions experiencing extremely rapid cooling/exhumation higher than several mm/yr e.g. New Zealand (Herman et al., 2010), eastern Himalayan syntaxis (King et al., 2016b), ESR thermochronometry could be much more widely applied.

10 The potential of ESR for thermochronometry has been recognized previously. Following from an earlier study (Ikeya, 1983), Toyoda and Ikeya (1991) first suggested that the intensity of quartz ESR centres could be used to determine the low-temperature thermal histories of the host rock. Scherer et al. (1993; 1994) investigated changing ESR centre intensities with depth through the known-thermal history KTB borehole in Germany (Coyle et al., 1997), which has also been used to validate
15 the luminescence thermochronometry technique (Guralnik et al., 2015, Biswas et al., 2018). Scherer et al. (1993; 1994) recorded a qualitative reduction in signal intensity of the Al-centre with increasing temperature and depth. In contrast, data for the Ti-centre were much more scattered with zero signal intensity recorded for many samples. However, it was Grün et al. (1999) who reported the first quantitative ESR-thermochronometry results from their study of the Eldzhurtinskiy Granite from the Russian Caucasus. Using the Al and Ti-centres of quartz, they obtained cooling rates of between 160 °C/Myr and 600
20 °C/Myr which correspond to denudation rates of ~2.5 and 5.5 mm/yr.

Despite the potential illustrated by ESR-thermochronometry in these early studies, the technique has not been applied since, in part associated with the difficulties of making ESR measurements (i.e. gamma or X-ray source availability, absence of automated instrumentation). In this study, we investigate the potential of ESR-thermochronometry through applying new
25 measurement protocols (Tsukamoto et al., 2015), which have been facilitated by developments in instrumentation (Oppermann and Tsukamoto, 2015), and that have recently been validated against samples with independent age control (Richter et al., In Press). We propose a kinetic model inspired by recent progress in luminescence thermochronometry (Lambert, ~~2018-et-al., In Review~~) to facilitate the inference of rock thermal histories from ESR laboratory data and perform a series of synthetic inversions to evaluate the range of cooling histories that ESR thermochronometry may be applicable over. We then investigate
30 six rock samples from the Japanese Alps and contrast their ESR thermal histories with those obtained from ~~paired~~-optically stimulated luminescence thermochronometry of feldspar (e.g. Guralnik et al., 2015; King et al., 2016b,c) of the same samples.

2. Theoretical basis

The theoretical basis of ESR-thermochronometry is very similar to that of luminescence thermochronometry (cf. King et al., 2016a; Herman and King, 2018 for reviews), with the advantage that unlike feldspar minerals, quartz minerals are not thought to suffer from athermal signal losses. Here we present the kinetic model for ESR-thermochronometry, before discussing how the parameters that describe signal growth and signal thermal decay can be constrained in the laboratory.

2.1 Kinetic model

We propose the following kinetic models to describe the evolution of ESR signals with temperature. A saturating system may be described by:

$$\frac{\partial \tilde{n}(E_a, t)}{\partial t} = \tilde{D}[1 - \tilde{n}(E_a, t)] - s e^{-\frac{E_a - \mu(E_a)}{k_B T}} [\tilde{n}(E_a, t)] \quad (1)$$

and a non-saturating system can be described by:

$$\frac{\partial \tilde{n}(E_a, t)}{\partial t} = \tilde{D}[\tilde{n}(E_a, t)] - s e^{-\frac{E_a - \mu(E_a)}{k_B T}} [\tilde{n}(E_a, t)] \quad (2)$$

15

where,

$$\tilde{n}(t) = \int_{E_a=0}^{\infty} P(E_a) \tilde{n}(E_a, t) dE_a \quad (3)$$

20 and,

$$P(E_a) = \frac{1}{\sigma(E_a)\sqrt{2\pi}} \exp\left(-\frac{1}{2}\left(\frac{E_a - \mu(E_a)}{\sigma(E_a)}\right)^2\right). \quad (4)$$

where \tilde{n} is the trapped charge population with activation energy, E_a (eV). In the instance of a saturating system \tilde{n} is expressed as a saturation ratio, but for a non-saturating system it is expressed as absorbed radiation dose (Gy). The first term on the right-hand side of Eqs. (1) and (2) describes charge trapping as a first-order process. For a non-saturating system, \tilde{D} is defined by the environmental dose rate \dot{D} (Gy), whereas for a saturating system, \tilde{D} is defined as \dot{D}/D_0 where D_0 is the characteristic dose of saturation (Gy). The second term on the right-hand side of Eqs. (1) and (2) describes thermal charge detrapping, and here we benefit from recent advances made in luminescence thermochronometry, and follow Lambert *et al.* (In-Review2018) by describing thermal detrapping using a model that assumes a Gaussian distribution of activation energies, E_a around the mean

trap depth, $\mu(E_t)$ (eV). Thermal detrapping is also described by the frequency factor, s (s^{-1}), the Boltzman constant, k_B (eV), temperature, T (K) and $P(E_a)$ the probability of thermally evicting electrons (or holes) from the trap (Eq. (4)). [An alternative approach could be to use a first or second order kinetic model as has been done previously \(Toyoda and Ikeya, 1991; Ikeya, 1993; Grün et al., 1999\) and we discuss our model selection more completely in the supplementary material.](#)

5

2.2 Constraining charge trapping

The natural trapped charge concentration, which reflects the equilibrium between charge trapping and thermally stimulated charge detrapping, can be measured in the laboratory through the development of a sample specific radiation dose response curve. This comprises measurement of a sample following increasingly large laboratory radiation doses, and interpolation of the natural ESR signal onto the resultant dose response curve. Measurements can either be made on single (e.g. Tsukamoto et al., 2015) or using multiple aliquots of the same sample (e.g. Grün et al., 1999). The former approach has only recently been made practical, following the introduction of X-ray irradiation for regenerative dosing (Oppermann and Tsukamoto, 2015). [as opposed to gamma irradiation which is often done at a laboratory separate to the measurement laboratory.](#)

10

2.3 Constraining charge detrapping

Thermal detrapping can be measured following laboratory isothermal decay experiments, whereby aliquots of a sample are given a radiation dose before being heated at different temperatures for different durations. The resultant signal loss is measured and fitted with the kinetic model described in Eqs. (1-4). Previous investigations have suggested that the thermal decay of quartz ESR can be described by first order or second order kinetics. Here, instead we use a density of states model, originally developed for the luminescence of feldspar (Li and Li, 2013; Lambert, 2018 et al., In Review; further details of model selection are given in the Supplementary Material). The selected model is based on a Gaussian distribution of activation energies $\sigma(E_t)$, around the mean trap-depth, $\mu(E_t)$ (Lambert, 2018 et al., In Review), and may be applicable for quartz ESR data where electrons can be trapped in a variety of different defects, e.g. $Ti^{3+} + e^-$ charge compensated by H^+ , Li^+ or Na^+ (Tsukamoto et al., 2018).

20

3. Assessing the potential of ESR-thermochronometry

Electron spin resonance dating analyses are not automated, meaning that the laboratory measurements required for ESR-thermochronometry analyses are considerably more time-consuming than those required for luminescence thermochronometry. It is thus necessary to verify that ESR-thermochronometry offers advantages over luminescence methods. To achieve this, a series of synthetic [inversions tests](#) for known cooling histories were done using the kinetic parameters of sample KRG16-06 (Table 1). [These tests first comprised running a forward model, which uses sample-specific kinetic parameters and a rate equation to describe signal growth. Through forward modelling, it is possible to predict the trapped-](#)

30

[charge concentration for a particular cooling history. The second stage of the test comprised inverting the trapped-charge concentrations predicted by the forward model, using the same rate equation, to determine if it is possible to recover the cooling history used in the forward model prediction. Further details of the forward and inverse modelling are given below.](#)

3.1 Forward modelling

5 Five different monotonic cooling scenarios were used to test the potential of ESR-thermochronometry in comparison to ~~OSL-~~
~~optically stimulated luminescence (OSL)~~ thermochronometry, comprising cooling with rates of 100 °C/Myr, 75 °C/Myr, 50
 °C/Myr, 25 °C/Myr and no cooling (i.e. isothermal holding at 0 °C for 2 Myr). All cooling rates were maintained for at least
 2 Myr with a starting temperature of 200 °C which is greater than the anticipated closure temperature of the ESR system (cf.
 Grün et al., 1999; Scherer, 1993; 1994). Using the kinetic model in Eqs. (1) and (2), a trapped charge population, \tilde{n}_{fwd} was
 10 predicted for both the Ti and Al-centres respectively using the kinetic parameters of sample KRG16-06 (Table 1) for the five
 different scenarios. In addition, the same exercise was carried out for four feldspar multi-OSL-thermochronometry signals of
 the same sample using the following kinetic model, after King et al., 2016a (see supplementary information for further details
 on model selection):

$$15 \frac{d\tilde{n}(r', E_b, t)}{dt} = \bar{D}[1 - \tilde{n}(r', E_{ab}, t)] - s e^{-\frac{E_t - E_b}{k_B T}} [\tilde{n}(r', E_b, t)] - \bar{s} e^{-\rho' r'^{-\frac{1}{3}}} [\tilde{n}(r', E_b, t)] \quad (5)$$

where the total accumulation of charge with time, i.e. $\tilde{n}(t)$ is obtained by integrating $\tilde{n}(r', E_b, t)$ over the range of band-tail
 states, E_b , and an infinite range of dimensionless distances, r' :

$$20 \tilde{n}(t) = \int_{r'=0}^{\infty} \int_{E_b=0}^{E_t} p(r') P(E_b) \tilde{n}(r', E_b, t) dE_b dr' \quad (6)$$

where $P(E_b)$ is the probability of evicting electrons into band-tail states of energy $E_b + dE_b$, defined as:

$$25 P(E_b) = B e^{-\left(-\frac{E_b}{E_w}\right)} dE_b \quad (7)$$

where B is a pre-exponential multiplier, and where $p(r')$ is the probability density distribution of the nearest recombination
 centre defined by Huntley (2006) as:

$$30 p(r') dr = 3r'^2 e^{-r'^3} dr' \quad (8)$$

where dimensionless distance $r' \equiv \left\{ \frac{4\pi\rho}{3} \right\}^{\frac{1}{3}} r$, the dimensionless density of recombination centres $\rho' \equiv \frac{4\pi\rho}{3\alpha^3}$ and α is a constant [related to the Bohr radius of the electron trap](#) (Huntley, 2006; Kars et al., 2008; Tachiya and Mozumder, 1974).

Table 1

5 3.2 Inverse modelling

We inverted the five sets of \tilde{n}_{fwd} values for the ESR and OSL data described above using a similar approach to King et al. (2016a), which we briefly outline here. The trapped-charge (or hole) populations were modelled for 10,000 randomly generated time-temperature histories (t-T paths), which were constrained to cool monotonically between 200 °C and 0±5 °C, over 2 Ma. We computed the dose response curves by solving the differential equations described above using a semi implicit Euler method (Press, 2007). For each t-T path we calculated a misfit between the [final](#) inverted trapped-charge population, \tilde{n}_{mod} , and our forward modelled values, \tilde{n}_{fwd} (Whelock et al., 2015), from which the misfit, M and likelihood, L are calculated:

$$M = \sum_1^m \left(0.5 \frac{\tilde{n}_{fwd}}{\sigma} \left(\log \left(\frac{\tilde{n}_{fwd}}{\tilde{n}_{mod}} \right) \right) \right)^2 \quad (9)$$

$$L = \exp(-M) \quad (10)$$

for m traps, where σ is the uncertainty. An arbitrary uncertainty on \tilde{n}_{fwd} of 10% was assumed. Cooling histories are then accepted or rejected by contrasting L with a random number between 0 and 1; if L is greater, the cooling history is retained. The accepted cooling histories are finally combined to construct a time-temperature history probability density function through dividing the time-temperature axis into 50 intervals and summing the number of paths that cross through each of the different cells. The Al, Ti and OSL data were first inverted separately and then the Al and Ti-centres were inverted together.

The results of the forward modelling and the synthetic inversions for the ESR and OSL data are shown in Fig. 1. The OSL signals for all cooling histories reach saturation (Fig. 1c), and this is reflected in the failure of the OSL to recover any of the cooling histories when inverted. [This is apparent because the 1σ confidence intervals show a broad range, with the highest density of cooling histories concentrated at temperatures < 20 °C over the past 500 ka indicating that the luminescence signals are saturated \(as shown in Fig. 1c\).](#) The minimum cooling rate that can be resolved using OSL for sample KRG16-06 is ~160 °C/Myr, calculated from 86% of the luminescence signal saturation level. Signal saturation is the key limitation that restricts the application of luminescence thermochronometry to regions undergoing rapid exhumation. In contrast, it is clear that the ESR data are able to resolve the 100 °C/Myr, 75 °C/Myr and 50 °C/Myr synthetic cooling histories [clearly](#), and cooling rates of 25 °C/Myr are distinct from isothermal holding at 0 °C over timescales of ~2 Ma. [This is apparent because of the coincidence](#)

between the prescribed cooling histories (white lines) and the highest density of accepted cooling histories shown by the brightest colours in the probability density functions. These results are significant as they show that ESR-thermochronometry is applicable in a range of geological settings beyond the rapidly exhuming locations that luminescence-thermochronometry is currently restricted to.

5

Figure 1

4. Proof of concept – Hida range, Japanese Alps

To further explore the potential of the ESR method we applied it to a suite of samples from the Hida range of the Japanese Alps. The Japanese Alps which reach elevations of up to 3,000 m are thought to have uplifted since the Pliocene or Quaternary (Yonekura et al., 2001; Tokahashi, 2006) in response to E-W compressional tectonic forces (Takahashi, 2006; Townend and Zoback, 2006; Sueoka et al., 2016). Lithology of the Hida range is dominated by granitic intrusions, including the Kurobegawa granite, which is the youngest known intrusion on Earth and which was emplaced between 10-0.8 Ma ago (Ito et al., 2013; 2017). Previous efforts to apply apatite fission-track dating on the Kurobegawa granite have been unsuccessful because of the very low fission-track density (Yamada, 1999). Extremely young apatite (0.50 ± 0.04 Ma) and zircon helium ages (0.37 ± 0.10 Ma) have recently been reported (Spencer et al., 2019), indicating that exhumation in this region has remained rapid throughout the Quaternary Period.

Six bedrock samples were taken from the Kurobegawa granite, northern Hida range of the Japanese Alps. Four surface samples were taken and form an elevation transect, whilst a further two samples were taken from a high-temperature tunnel, which has a present-day temperature of ~40-50 °C but which had temperatures of up to 165 °C at the time of excavation in the late 1930s (Yuhara and Yamamoto, 1983). Samples had a minimum size of 15 x 15 x 15 cm, to ensure that a light safe portion could be extracted from their interiors. Sample details are given in the Supplementary Material.

4.1 Sample preparation

Bedrock samples were prepared using standard laboratory methods under subdued red light conditions at the University of Lausanne and University of Bern, Switzerland (cf. King et al., 2016c). At least 10 mm was cut from the exterior of the samples using a water-cooled diamond saw, to extract the light safe interior. A thin section was made using a representative sample of the bedrock exterior and a further representative sample was sent to ActLabs, Canada for ICP-MS analysis. Sample interiors were then hand crushed to extract the 180-212 µm grain size fraction, which was treated with HCl and H₂O₂ to remove any carbonates and organic material respectively. The K-feldspar and quartz fractions were separated from heavy minerals using heavy liquids. The K-feldspars were retained for luminescence dating, whilst the quartz extracts ($2.58 > \rho < 2.70$ g cm⁻³) were etched for 40 minutes using 40% HF, before being treated with HCl to remove fluorides that had precipitated during etching.

The etched samples were sieved to $>150\ \mu\text{m}$, to remove any partially dissolved feldspar grains. Aliquots for ESR measurement comprised 60 mg of quartz loaded into glass tubes with interior and exterior diameters of 2 and 3 mm respectively.

4.2 Environmental dose rate determination

5 The grain size distribution of quartz and feldspar minerals within the parent bedrock was estimated from thin section analysis using the software of Buscombe (2013). The environmental dose rate, \dot{D} , was calculated from the sample specific radioisotope concentrations using DRAC v.1.2 (Durcan et al., 2015), the conversion factors of Guérin et al. (2011), the alpha grain size attenuation factors of Bell (1980) and the beta grain size attenuation factors of Guérin et al. (2012). Because the bedrock samples have only been at the surface for a short period of time, no cosmic dose rate was included in the calculation. The water content was estimated at $2 \pm 2\%$. For the quartz extract, an etch depth of $10\ \mu\text{m}$ was assumed and the alpha dose rate adjusted following Bell (1980); an a-value of 0.040 ± 0.005 was used after Rees-Jones (1995) for any residual alpha dose. No internal dose rate was included. In contrast, the feldspar fraction was not etched, and an a-value of 0.15 ± 0.05 was used after Balescu and Lamothe (1994). An internal K-content of $12.5 \pm 5.0\%$ was assumed following Huntley and Baril (1997). The calculated environmental dose rates are summarized in Table 1 and full calculation details are given in the Supplementary Material.

4.3 Electron Spin Resonance

15 Electron Spin Resonance measurements were done at the Leibniz Institute for Applied Geophysics in Hannover, Germany. Measurements were made on a JEOL JES-FA100 spectrometer using 2.0 mW microwave power, 0.1 mT modulation width, a $333.5 \pm 15\ \text{mT}$ magnetic field, 0.1 s time constant and 60 s scan which was averaged over 3 scans. All spectra were measured 3 times following sample turning by 60° to avoid any anisotropic effects. Measurements were made at $-150\ ^\circ\text{C}$. The instrumentation detailed in Oppermann and Tsukamoto (2015) was used to facilitate X-ray irradiation and sample preheating, which is described below. The Ti and Al-centre peaks were fitted using V3.3.35 of the JEOL ESR data processing software, and were normalized relative to the intensity of the 6th hyperfine line of Mn^{2+} from the internal MgO standard, doped with MnO. As our measurements were carried out at $-150\ ^\circ\text{C}$, it was not possible to differentiate between the Ti-H and Ti-Li centres, and consequently they have been treated as a single centre (Fig. 2). All subsequent data fitting was done using MATLAB.

25 *Figure 2*

Formatted: Font: Italic

4.3.1 Measurement protocol optimization

Tsukamoto et al. (2015; 2018) recently showed that it is necessary to preheat ESR samples that are measured in a single aliquot protocol to avoid any signal contribution from trapped charge that is unstable over laboratory timescales, similar to luminescence dating (cf. Murray and Wintle, 2000). Within this study, a series of tests were done to select the most appropriate preheat temperature and duration. The signal intensities of five aliquots of samples KRG16-06 and KRG16-104 were measured following different preheat treatments (i.e. one aliquot per temperature; Fig. 2a3a). Aliquots of KRG16-06 were preheated for

two minutes at temperatures of between 160 °C and 240 °C, whereas aliquots of sample KRG16-104 were preheated for four minutes at temperatures of between 120 °C and 200 °C. The signal intensity of a further aliquot of each sample was measured without laboratory preheating. In addition to measuring the ESR signal intensity, the equivalent doses of the Ti and Al-centres of KRG16-06 for each preheat temperature, were measured in a single aliquot method (Tsukamoto et al., 2015; Fig. 2b3b).

5 The single aliquot protocol comprised measurement of the natural signal, measurement of a single additive dose, annealing at 420 °C for two minutes and measurement following zero dose. All irradiations were given using an X-ray source with a dose rate of ~0.3 Gy s⁻¹ (Tsukamoto et al., 2018); aliquots were manually turned once during irradiation to ensure that even dosing was achieved.

10 **Figure 23**

4.3.2 Measurement of the trapped charge concentration

The trapped charge population of the different samples was measured using a single aliquot approach. This comprised measurement of the natural signal, a zero-point measurement following annealing of the aliquot at 380 °C for four minutes, and measurement of two or three regenerative doses points. The natural signal was then interpolated onto the dose response curve to determine the equivalent dose; all equivalent dose values were calculated using a linear fit. To confirm that the measurement protocol was appropriate, a dose-recovery experiment was done. Three aliquots of zero-age sample KRG16-112 were given an X-ray dose of 360 Gy, before measurement using the same protocol outlined above. Trapped-charge dating systems usually experience signal saturation, therefore it is also necessary to constrain the form of ESR centre dose response. Using a new aliquot of each sample, dose response was measured using the same measurement protocol, but omitting the zero-point measurement step, [i.e. in an additive dose response protocol](#).

4.3.3 Measurement of trapped charge thermal decay

Thermal signal losses were measured using an isothermal decay experiment, whereby three aliquots of each sample were irradiated with an additive dose of 4.30 kGy. The aliquots were then preheated at 160 °C for four minutes prior to initial measurement, and were then measured following isothermal holding at between 130 °C and 180 °C for 4, 8, 16, 32, 64, 128 and 256 minutes. This experiment was also repeated on three fresh aliquots of sample KRG16-104 using a smaller dose of 2.15 kGy.

4.4 OSL measurements

OSL measurements of all samples followed the approach of King et al. (2016b,c). Luminescence measurements were made at the University of Bern using a single aliquot regenerative dose multiple-elevated-temperature (MET) infra-red stimulated luminescence (IRSL) measurement protocol (Li and Li, 2011) comprising a preheat at 250 °C for 60 seconds, followed by four IRSL measurements at 50, 100, 150 and 225 °C each of 100 s duration. A test dose of 160 Gy was used, which is c. 30% of

the IRSL₅₀ signal equivalent dose value of samples KRG16-06, KRG16-101 and KRG16-104. Each measurement cycle was followed by a high temperature optical wash at 290 °C for 60 s. Regenerative doses up to ~4.50 kGy were given to three small (2 mm diameter) aliquots of each sample using two different Risø TL-DA-20 luminescence readers with dose rates ranging from 0.06 to 0.10 Gy s⁻¹ dependent on instrument (dose rates are provided for each measurement in the Supplementary Materials). Luminescence signals were detected in the blue part of the visible spectrum using a BG39 and BG3 or Corning 7-59 filter combination. The suitability of the selected measurement protocol was confirmed using a dose recovery test.

Rates of athermal and thermal charge detrapping were also measured using a single aliquot regenerative dose method on the same aliquots used to measure the luminescence dose response curve. Athermal detrapping rates were quantified at room temperature by measuring the luminescence response to a fixed dose following different delay periods. Aliquots were preheated prior to storage following Auclair et al. (2003) and maximum fading delays were 122 days. Rates of thermal charge detrapping were measured using isothermal holding experiments. The aliquots were given a dose of 50 Gy, and held at temperatures ranging from 170 to 350 °C for delay times of 0 to 10,240 s prior to measurement.

5. Results

5.1 Electron Spin Resonance

The signal intensity experiment indicates a plateau for the Ti-centre of sample KRG16-104 up until 160 °C (Fig. 2a3a). In contrast, the Al-centre for this sample and the Ti-centre of sample KRG16-06 reduce in intensity by ~5% between room temperature and 160 °C whilst the Al-centre of sample KRG16-06 is depleted further, by ~10%. The signal intensity data for KRG16-06 are relatively noisy (non-monotonic signal decay with increasing preheat temperature) in comparison to KRG16-104. However, in spite of this, within the preheat-plateau experiment (Fig. 2b3b), a plateau in D_e values between 160 and 220 °C is recorded for this sample following preheating for two minutes. On the basis of these experiments a preheat temperature of 160 °C was selected as this temperature maximises signal intensity (Fig. 3a) whilst remaining within the D_e value plateau (Fig. 3b).

Preheating for short durations resulted in the heater unit overshooting the target temperature and poor thermal reproducibility. For this reason, a longer duration preheat at 160 °C for four minutes was selected for all measurements. This selected protocol is further validated by the successful recovery of a 360 Gy dose from naturally zero-age sample KRG16-112 for both the Al and Ti-centres, which yield recovered to given dose ratios of 0.83 ± 0.20 and 1.01 ± 0.06 respectively (n=3).

Measurements of the trapped charge population of the Al and Ti-centres were similar between aliquots resulting in 1σ uncertainties of ~20%. Equivalent dose values for the Al- and Ti-centres were within uncertainty for all samples, and ages ranged from $247-291 \pm 54-13$ ka for sample KRG16-05 to $37 \pm 4-2$ ka for sample KRG16-104 (Table 1). Samples KRG16-111

and KRG16-112 from the high-temperature tunnel yielded zero age; consequently, full dose response and isothermal decay was not measured for sample KRG16-112 [and it is not included in Table 1](#). Whereas it was possible to saturate the Ti-centre of all samples with the maximum given dose of 19 kGy, the Al-centre continued to grow linearly throughout measurement for all samples (Fig. [3a4a,c](#)). Continued growth of the Al-centre has been reported previously and has been accommodated through fitting dose response with an exponential plus linear function (e.g. Duval, 2012). In contrast, for the KRG samples, the Al-centre is best described using a linear regression (Fig. [3a4a](#)). In contrast, the Ti-centre of all samples showed a reduction in signal intensity at high doses (i.e. >10 kGy), which has also been reported previously (e.g. Duval and Guilarte, 2015) and has been attributed to changing electron capture probabilities (Woda and Wagner, 2007). To characterise the maximum possible trapped-charge population we excluded data points where the ESR signal intensity started to reduce (white data points in Fig. [3e4c](#)) and fitted the remaining data with a single saturating exponential function (e.g. Grün and Rhodes, 1991) of the form:

$$\tilde{n} \approx \frac{I}{I_{sat}} = \left(1 - e^{-\frac{D+D_e}{D_0}}\right) \quad (11)$$

where I is the natural ESR signal intensity, I_{sat} is the saturation intensity of the ESR signal and D is the given dose (Gy). Because the Ti-centre experiences saturation, the equivalent dose value, D_e , can also be expressed as a saturation ratio, i.e. $\tilde{n} = (n/N)$. As only a single aliquot of each sample was dosed until saturation, \tilde{n} values for the Ti-centre were calculated from interpolation of the average D_e value ($n=3$) onto the single dose response curve, thus \tilde{n} values for the Ti-centre are derived from multiple aliquots.

Toyoda and Ikeya (1991) suggested that the thermal decay of the E' , Al and Ti-centres follows second order kinetics, however it was not possible to fit our data using either a first or second order kinetic model (Supplementary Material). Instead the isothermal decay data were fitted using a multiple first order kinetic model (Lambert, [2018-et-al., In-Review](#); Table 1). Whilst the actual physical meaning of a Gaussian distribution of energies requires further investigation within the context of ESR defects, and it is unlikely that both the Al and Ti-centres follow exactly the same process of thermal decay, preliminary fits to the data using this model are promising (Fig. [3b4b,d](#)). Values of $\mu(E_i)$ ranged from 1.3 – 1.9 eV between samples and centres (Table 1).

Figure 34

5.2 Optically Stimulated Luminescence

For all of the samples, the measured luminescence signals fulfilled the acceptance criteria (see Supplementary Material for further details). The IRSL₅₀ signals of all samples exhibited very high rates of fading with g_{2days} values ranging from 6-11

%/decade, whereas for post-IR IRSL measurements at 225 °C, fading rates were 2-4 %/decade. The model introduced by Huntley (2006) was used to fit the athermal detrapping data to determine ρ' . Using this model to fading correct the trapped charge concentrations following Kars et al. (2008) indicates that the IRSL₅₀ signals of samples KRG16-06 and KRG16-101, and all signals for sample KRG16-05 are saturated (see Supplementary Material). All other signals can be used to determine rock-cooling histories. Saturation of the IRSL₅₀ signals relative to the higher temperature signals is a consequence of their relatively high rate of anomalous fading. The luminescence dose response data of all of the samples and signals were fitted with a single saturating exponential fit to determine the characteristic dose of saturation, D_0 and the concentration of trapped charge, \bar{n} . Although for some samples a general order kinetic model (GOK) fit would result in lower deviation from the measured values, GOK fits have been shown to overestimate sample athermal field saturation values (King et al., 2018), which must be done accurately to evaluate if a sample contains thermal information (cf. Valla et al., 2016). Finally, the isothermal decay data were fitted using the band-tail states model (Poolton et al., 2009; Li and Li, 2013; Eq. 6 and 7) to determine E_i , E_u and s . Values of E_i ranged from 1.2 – 1.5 eV between samples and signals (Table 2).

5.3 Inversion of ESR and OSL data for cooling histories

In order to invert the data into cooling histories, we used the same approach outlined in section 3. We computed OSL and ESR dose response curves from 10,000 randomly generated t-T paths, which were constrained to cool monotonically between 200 °C and 15 ± 5 °C, over 2 Ma. Initially the Al-centre, Ti-centre and OSL centres were inverted separately, before being inverted together. The results for all samples with the exception of naturally zero-age samples KRG16-111 and KRG16-112, are shown in Fig. 45.

Figure 45

6. Discussion

Trapped-charge thermochronometers offer benefits over other thermochronometry systems because of their low closure temperature and ability to yield precise cooling histories over Quaternary timescales (Herman and King, 2018). However, signal saturation has proven a significant barrier to the application of luminescence thermochronometry (cf. Valla et al., 2016). For ESR thermochronometry to offer a viable alternative it should exhibit later signal saturation but also similar thermal stability. The measurements presented here are promising because whilst the ages measured for the OSL and ESR systems are similar, the maximum possible ages that can be obtained from the ESR Ti-centre are more than four times greater than the maximum possible age that can be obtained from the OSL signals (Tables 1 and 2). Furthermore, the Al-centre of the KRG samples does not exhibit signal saturation up to 19 kGy, which was the maximum dose explored in this study (Fig. 3a4a). Although such linear dose response behaviour has, to our knowledge, not been reported previously and thus may be a property

of these exceptionally young quartz minerals, it is an exciting observation that warrants further study through the investigation of further quartz samples.

5 Samples KRG16-111 and KRG16-112 from the high temperature tunnel yielded zero, or near-zero ages for both ESR centres and the IRSL signals investigated (Tables 1 and 2). These samples provide an important local control on the thermal stability of these trapped-charge systems, demonstrating that all charge is evicted from the centres at sufficiently high temperatures. For the remaining samples, the ages obtained from the two ESR centres are within uncertainties, indicating that they may have similar thermal stability. For the OSL data, some variance in age is recorded between the different signals (Table 2); all signals of sample KRG16-05 are in field saturation, and thus only a minimum sample age of ~180 ka can be calculated (Table 2). The 10 IRSL₅₀ signals of samples KRG16-06 and KRG16-101 are also in field saturation, yielding the highest apparent ages for these samples, and are not considered further. For samples KRG16-06 and KRG16-101, the remaining IRSL signals show a general reduction in age with increasing stimulation temperature, possibly indicating that the ages have been overcorrected for anomalous fading using the Huntley (2006) model (cf. King et al., 2018). The OSL and ESR ages of samples KRG16-06 and KRG16-104 are similar, indicating that for these samples the ESR and OSL signals have similar thermal stability, and thus 15 that ESR-thermochronometry would also be suitable for resolving late stage cooling histories. In contrast, sample KRG16-101 yields OSL ages twice as large as the ESR ages, which could be indicative of a difference in centre thermal stability.

To further evaluate the relative thermal stability of the ESR and OSL signals, the isothermal decay of the ESR and feldspar systems was simulated using the experimentally constrained kinetic parameters of the different samples, for isothermal 20 conditions of 20 °C assuming an initial trapped charge concentration of 1 and assuming no charge trapping (Fig. 56). Note that anomalous fading related signal loss has also been included for the OSL signals, as excluding this variable would result in erroneously high apparent signal stabilities. The ESR centres have similar thermal stability to the IRSL centres for all samples, with the exception of sample KRG16-101 (Figs. 56c) where the ESR centres are more thermally stable. The Ti-centre is more thermally stable than the Al-centre for all samples, with the exception of sample KRG16-104 for the measurement in response 25 to 2.15 kGy. This is consistent with the earlier work of Grün et al. (1999) who also extracted quartz from granitic bedrock and observed that the Ti-centre is more thermally stable than the Al-centre, but contrasts with observations from Chinese loess (Tsukamoto et al., 2018). The contrasting behaviour between the two measurements of KRG16-104 in response to doses of 4.30 kGy and 2.15 kGy (Fig. 56d) reflects uncertainty in the derivation of ESR kinetic parameters, potentially related to inter-aliquot variability. Improved measurement protocols and the development of automated instrumentation may alleviate these 30 discrepancies through improving measurement reproducibility, however despite this, the thermal stability determined in both experiments is broadly similar (Fig. 56d). The general trend of ESR signals exhibiting similar thermal stability to IRSL signals indicates that ESR-thermochronometry will record changes in exhumation histories from a similar thermal range as OSL-thermochronometry, whilst benefitting from considerably later signal saturation and being unaffected by anomalous fading.

Figure 56

Inverting the Al and Ti-centres of all samples results in broadly similar time-temperature histories between centres, whilst the cooling histories of different samples vary (Fig. 45). This is in agreement with the Al and Ti-centres' similar thermal stabilities (Fig. 56) and measured ages (Table 1). The two different centres can also be effectively combined to produce a single cooling history (Fig. 45), which is similar to that inverted from the OSL data alone for samples KRG16-101 and KRG16-104 (Fig. 45). For sample KRG16-05, the saturated OSL signals result in a broad cooling history, whereas for sample KRG16-06 the OSL data yield more rapid cooling than the ESR data. The OSL and ESR data can also be inverted together. These data show that for samples beyond the range of OSL dating, ESR-thermochronometry will be able to provide cooling histories over a similar thermal range, allowing late stage exhumation histories to be determined. The data inversions reveal that rates of rock cooling in the Hida range of the Japanese Alps are consistent with previous investigations [that indicate rapid rock cooling](#)-(Ito et al., 2013; 2017; Spencer et al., 2019). Whereas sample KRG16-05 experienced almost no cooling over the past 2 Myr, cooling rates accelerated from ~100 °C/Myr (calculated from the U/Pb ages of Ito et al., 2013) to rates of >400°C/Myr over the past 100 ka for samples KRG16-06, KRG16-101 and KRG16-104.

7. Conclusions and Outlook

In this study, the potential of ESR thermochronometry for constraining rates of rock cooling has been explored for a suite of samples from the Hida range of the Japanese Alps. Through using the latest ESR measurement protocols (Tsukamoto et al., 2015) and instrumentation (Oppermann and Tsukamoto, 2015) the dose response and thermal stability of both the Al and Ti-centres has been constrained. Whilst the Ti-centre can be described with a single saturating dose response curve, the Al-centre continues to grow linearly with laboratory irradiation. A multiple-first order model based on a distribution of trap-depths was successfully used to fit isothermal decay data (Lambert, [2018 et al., In Review](#)), which do not follow either simple first-order, or second-order decay. Contrasting the thermal stability of the Al and Ti-centres with that of the luminescence centres of feldspar shows that the ESR of quartz has similar thermal stability. The Al and Ti-centres can be successfully inverted together for rock cooling for all of the samples investigated. It was also possible to invert the OSL and ESR data together for all samples analysed, providing further constraints on their thermal histories. Whereas OSL-thermochronometry of sample KRG16-06 can only recover a minimum cooling rate of ~160 °C/Myr, both ESR centres have the potential to recover cooling rates of as low as 50-25 °C/Myr, illustrating the potential of ESR for resolving late-stage cooling histories.

Acknowledgements

GEK acknowledges financial support from a Mobility Grant from the University of Cologne that funded initial fieldwork and from Swiss National Science Foundation (SNSF) grant number PZ00P2_167960. SS and TT

acknowledge support from the Grant-in-Aid for Scientific Research on Innovative Areas (KAKENHI No. 26109003) from the Ministry of Education, Culture, Sports, Science and Technology (MEXT). We thank the Chubu Regional Environment Office for permission to collect rocks in the Chubu Sangaku National Park. Sample collection was supported by the Kansai Electric Power Co., Inc., Y. Hino (KANSO Co., Ltd.), Dr. T. Komatsu (JAEA), S. Terusawa (OYO Co., Ltd.), S. Fukuda, T. Arai (Kyoto Univ.), and staff of the Azohara lodge. The Herbetta Foundation funded ST to stay at the University of Lausanne during the study. Benny Guralnik is thanked for commenting on an earlier version of this manuscript.

References

- Auclair, M., Lamothe, M. and Huot, S., 2003. Measurement of anomalous fading for feldspar IRSL using SAR. Radiation measurements, 37(4-5), pp.487-492.
- Balescu, S. and Lamothe, M., 1994. Comparison of TL and IRSL age estimates of feldspar coarse grains from waterlain sediments. Quaternary Science Reviews, 13(5-7), pp.437-444.
- Bell, W.T., 1980. Alpha dose attenuation in quartz grains for thermoluminescence dating. Ancient TL, 12(4), p.8.
- Biswas, R., Herman, F., King, G.E., Braun, J., 2018. Thermoluminescence of feldspar as a multi-thermochronometer to constrain the temporal variation of rock exhumation in the recent past. Earth and Planetary Science Letters 495, 56-68.
- Buscombe, D. (2013). Transferable wavelet method for grain-size distribution from images of sediment surfaces and thin sections, and other natural granular patterns. Sedimentology, 60(7), 1709-1732.
- Coyle, D. A., Wagner, G. A., Hejl, E., Brown, R., & Van den Haute, P. (1997). The Cretaceous and younger thermal history of the KTB site (Germany): apatite fission-track data from the Vorbohrung. Geologische Rundschau, 86(1), 203-209.
- Durcan, J.A., King, G.E. and Duller, G.A., 2015. DRAC: Dose Rate and Age Calculator for trapped charge dating. Quaternary Geochronology, 28, pp.54-61.
- Duval, M., 2012. Dose response curve of the ESR signal of the Aluminum center in quartz grains extracted from sediment. Ancient TL, 30(2), pp.41-49.
- Duval, M. and Guilarte, V., 2015. ESR dosimetry of optically bleached quartz grains extracted from Plio-Quaternary sediment: evaluating some key aspects of the ESR signals associated to the Ti-centers. Radiation Measurements, 78, pp.28-41.
- Grün, R., 1989. Electron spin resonance (ESR) dating. Quaternary International, 1, pp.65-109.
- Grün, R., Rhodes, E.J., 1991. On the selection of dose points for saturating exponential ESR/TL dose response curves. Ancient TL 9, 40-46.
- Grün, R., Tani, A., Gurbanov, A., Koshchug, D., Williams, I., & Braun, J. (1999). A new method for the estimation of cooling and denudation rates using paramagnetic centers in quartz: A case study on the Eldzhurtinskiy Granite, Caucasus. Journal of Geophysical Research: Solid Earth, 104(B8), 17531-17549.
- Guérin, G., Mercier, N. and Adamiec, G., 2011. Dose-rate conversion factors: update. Ancient TL, 29(1), pp.5-8.

- Guérin, G., Mercier, N., Nathan, R., Adamiec, G., & Lefrais, Y. (2012). On the use of the infinite matrix assumption and associated concepts: a critical review. *Radiation Measurements*, 47(9), 778-785.
- Guralnik, B., Jain, M., Herman, F., Ankjærgaard, C., Murray, A.S., Valla, P.G., Preusser, F., King, G.E., Chen, R., Lowick, S.E., Kook, M., Rhodes, E.J., 2015. OSL-thermochronology of feldspar from the KTB borehole, Germany. *Earth and Planetary Science Letters* 423, 232-243.
- 5 Herman, F., Rhodes, E.J., Braun, J., Heiniger, L., 2010. Uniform erosion rates and relief amplitude during glacial cycles in the Southern Alps of New Zealand, as revealed from OSL-thermochronology. *Earth and Planetary Science Letters* 297 (1-2), 183-189.
- Herman, F. and King, G.E., 2018. Luminescence Thermochronometry: Investigating the Link between Mountain Erosion, Tectonics and Climate. *Elements: An International Magazine of Mineralogy, Geochemistry, and Petrology*, 14(1), pp.33-38.
- 10 Huntley, D.J. and Baril, M.R., 1997. The K content of the K-feldspars being measured in optical dating or in thermoluminescence dating. *Ancient TL*, 15(1), pp.11-13.
- Huntley, D.J., 2006. An explanation of the power-law decay of luminescence. *Journal of Physics: Condensed Matter* 18(4), 1359-1365.
- 15 Ikeya, M., 1983. ESR studies of geothermal boring cores at Hachobara power station. *Japanese Journal of Applied Physics*, 22(12A), p.L763.
- Ikeya, M., 1993. *New applications of electron spin resonance: dating, dosimetry and microscopy*. World Scientific.
- Isoya, J., Weil, J. A., & Davis, P. H. (1983). EPR of atomic hydrogen 1H and 2H in α -quartz. *Journal of Physics and Chemistry of Solids*, 44(4), 335-343.
- 20 Ito, H., Yamada, R., Tamura, A., Arai, S., Horie, K. and Hokada, T., 2013. Earth's youngest exposed granite and its tectonic implications: the 10–0.8 Ma Kurobegawa Granite. *Scientific reports*, 3, p.1306.
- Ito, H., Spencer, C. J., Danišik, M., & Hoiland, C. W. (2017). Magmatic tempo of Earth's youngest exposed plutons as revealed by detrital zircon U-Pb geochronology. *Scientific Reports*, 7(1), 12,457.
- Kars, R.H., Wallinga, J., and Cohen, K.M., 2008. A new approach towards anomalous fading-correction for feldspar IRSL dating-tests on samples in field saturation. *Radiation Measurements* 43(2), 786-790.
- 25 King, G.E., Guralnik, B., Valla, P.G. and Herman, F., 2016a. Trapped-charge thermochronometry and thermometry: A status review. *Chemical Geology*, 446, pp.3-17.
- King, G.E., Herman, F., & Guralnik, B., 2016b. Northward migration of the eastern Himalayan syntaxis revealed by OSL thermochronometry. *Science*, 353(6301), 800-804.
- 30 King, G.E., Herman, F., Lambert, R., Valla, P. G., & Guralnik, B. (2016c). Multi-OSL-thermochronometry of feldspar. *Quaternary Geochronology*, 33, 76-87.
- King, G.E., Burow, C., Roberts, H.M.R. & Pearce, N.J.P., [Accepted 2018](#). Age determination using feldspar: evaluating fading-correction model performance. *Radiation Measurements*, [119, 55-73](#).

- ~~Lambert, R., King, G.E., Valla, P., Herman, F., In Review. Validating multiple first-order kinetic models for feldspar thermal decay in luminescence thermochronometry. Radiation Measurements.~~
- ~~Lambert, R. 2018. Investigating thermal decay in K-feldspar for the application of IRSL thermochronometry on the Mont Blanc massif. Unpublished PhD Thesis, University of Lausanne, Switzerland.~~
- 5 Li, B. and Li, S.H., 2011. Luminescence dating of K-feldspar from sediments: a protocol without anomalous fading correction. *Quaternary Geochronology*, 6(5), pp.468-479.
- Li, B. and Li, S.H., 2013. The effect of band-tail states on the thermal stability of the infrared stimulated luminescence from K-feldspar. *Journal of Luminescence*, 136, pp.5-10.
- ~~Murray, A.S., Wintle, A.G., 2000. Luminescence dating of quartz using an improved single-aliquot regenerative-dose protocol. Radiation Measurements 32(1), pp.57-73.~~
- 10 Nuttall, R.H.D. and Weil, J.A., 1981. The magnetic properties of the oxygen-hole aluminum centers in crystalline SiO₂. I.[AlO4]^o. *Canadian Journal of Physics*, 59(11), pp.1696-1708.
- Oppermann, F. and Tsukamoto, S., 2015. A portable system of X-ray irradiation and heating for electron spin resonance (ESR) dating. *Anc. TL*, 33, pp.11-15.
- 15 Poolton, N.R.J., Kars, R.H., Wallinga, J. and Bos, A.J.J., 2009. Direct evidence for the participation of band-tails and excited-state tunnelling in the luminescence of irradiated feldspars. *Journal of Physics: Condensed Matter*, 21(48), p.485505.
- Press, W.H., 2007. *Numerical Recipes 3rd Edition: the Art of Scientific Computing*. Cambridge University Press.
- Rees-Jones, J., 1995. Optical dating of young sediments using fine-grain quartz. *Ancient TL* 13 (2), 9-14.
- Rinneberg, H., & Weil, J. A. (1972). EPR Studies of Ti³⁺-H⁺ Centers in X-Irradiated α -Quartz. *The Journal of Chemical Physics*, 56(5), 2019-2028.
- 20 Richter, M., Tsukamoto, S., Long, H. (In Press). ESR dating of Chinese loess using the quartz Ti centre: A comparison with independent age control. *Quaternary International*. <https://doi.org/10.1016/j.quaint.2019.04.003>
- Rink, W.J., 1997. Electron spin resonance (ESR) dating and ESR applications in Quaternary science and archaeometry. *Radiation Measurements*, 27(5-6), pp.975-1025.
- 25 Scherer, T., Agel, A., Hafner S.S., 1993. Determination of uplift rates using ESR investigations of quartz, KTB Rep. 93-2. Kontinentales Tiefbohrprogramm der Bundesrepublik Deutschland Niedersächs. Landesamt Bodenforsch., Hannover, 121- 124.
- Scherer, T., Plötze, M., Hafner, S.S., 1994. Paramagnetic defects of quartz in KTB and a drilling profile from Eldzhurtinskiy Granite, Russia. KTB Rep. 94-2. B25, Kontinentales Tiefbohrprogramm der Bundesrepublik Deutschland Niedersächs. Landesamt Bodenforsch., Hannover.
- 30 Spencer, C.J., Danišik, M., Ito, H., Hoiland, C., Tapster, S., Jeon, H., McDonald, B. and Evans, N.J., 2019. Rapid exhumation of Earth's youngest exposed granites driven by subduction of an oceanic arc. *Geophysical Research Letters*.
- Sueoka, S., Tsutsumi, H. and Tagami, T., 2016. New approach to resolve the amount of Quaternary uplift and associated denudation of the mountain ranges in the Japanese Islands. *Geoscience Frontiers*, 7(2), pp.197-210.

- Tachiya, M., and Mozumder, A., 1974. Decay of trapped electrons by tunnelling to scavenger molecules in low temperature glasses. *Chemical Physics Letters* 28(1), 87-89.
- Takahashi, M., 2006. Tectonic Development of the Japanese Islands Controlled by Philippine Sea Plate Motion. *Journal of Geography (Chigaku Zasshi)* 115, 116-123. (in Japanese with English Abstract)
- 5 Tissoux, H., Falguères, C., Voinchet, P., Toyoda, S., Bahain, J. J., and Despriée, J., 2007. Potential use of Ti-center in ESR dating of fluvial sediment. *Quaternary Geochronology*, 2(1-4), 367-372.
- Townend, J., Zoback, M.D., 2006. Stress, strain, and mountain building in central Japan. *Journal of Geophysical Research: Solid Earth (1978–2012)* 111.
- Toyoda, S. and Ikeya, M., 1991. Thermal stabilities of paramagnetic defect and impurity centers in quartz: Basis for ESR dating of thermal history. *Geochemical Journal*, 25(6), pp.437-445.
- 10 Tsukamoto, S., Toyoda, S., Tani, A., & Oppermann, F., 2015. Single aliquot regenerative dose method for ESR dating using X-ray irradiation and preheat. *Radiation Measurements*, 81, 9-15.
- Tsukamoto, S., Long, H., Richter, M., Li, Y., King, G.E., He, Z., Yang, L., Zhang, J. and Lambert, R., 2018. Quartz natural and laboratory ESR dose response curves: A first attempt from Chinese loess. *Radiation Measurements*.
- 15 Valla, P.G., Lowick, S.E., Herman, F., Champagnac, J.D., Steer, P. and Guralnik, B., 2016. Exploring IRSL50 fading variability in bedrock feldspars and implications for OSL thermochronometry. *Quaternary Geochronology*, 36, pp.55-66.
- Wheelock, B., Constable, S., Key, K., 2015. The advantages of logarithmically scaled data for electromagnetic inversion. *Geophysical Journal International* 201, 1765-1780.
- Woda, C., Wagner, G. A., 2007. Non-monotonic dose dependence of the Ge-and Ti-centres in quartz. *Radiation Measurements*, 42(9), 1441-1452.
- 20 Yamada, R. (1999) Cooling history analysis of granitic rock in the Northern Alps, central Japan. *The Earth Monthly*, 21, 803–810 (in Japanese).
- Yonekura, N., Kaizuga, S., Nogami, M., Chinzei, K., 2001. Introduction to Japanese geomorphology. University of Tokyo Press, Tokyo. (in Japanese)
- 25 Yuhara, K. and Yamamoto, T., 1983. Thermal Effect of Water Flowing through Fractures on the Cooling of Kurobe Jobu Railway Tunnel (Hot Tunnel), Central Japan. *Journal of the Geothermal Research Society of Japan*, 5(4), pp.259-276.

Table 1: ESR centre kinetic parameters, D_e values and ages. Maximum ages are calculated from 2^*D_e . Full details of environmental dose rate derivation are given in the Supplementary Material.

Ti-Centre	\dot{D} (Gy ka ⁻¹)	D_0 (Gy)	$\mu(E_T)$ (eV)	$\log_{10}(s)$ (s ⁻¹)	$\sigma(E_T)$ (eV)	\bar{n}	D_e (Gy)	Age (ka)	Maximum Age (Ma)
KRG16-05	6.37 ± 0.38	2,555 ± 438	1.44 ± 0.10	12.72 ± 1.11	0.09 ± 0.01	0.50 ± 0.02	1,859 ± 81	291 ± 13	0.82
KRG16-06	3.60 ± 0.13	3,182 ± 607	1.79 ± 0.10	17.16 ± 1.15	0.12 ± 0.01	0.20 ± 0.02	275 ± 24	76 ± 7	1.77
KRG16-101	3.97 ± 0.33	2,495 ± 249	1.89 ± 0.15	17.88 ± 1.74	0.13 ± 0.01	0.10 ± 0.00	145 ± 6	37 ± 2	1.29
KRG16-104	4.42 ± 0.23	2,804 ± 302	1.70 ± 0.15	15.42 ± 1.64	0.10 ± 0.01	0.16 ± 0.01	334 ± 15	76 ± 4	1.34

KRG16-111 4.54 ± 0.42 2,915 ± 172 1.69 ± 0.07 15.89 ± 0.78 0.11 ± 0.01 0.00 ± 0.00 - 4.76 ± 11.3* 1.28

Al-Centre

KRG16-05	6.37 ± 0.38	-	1.27 ± 0.05	10.82 ± 0.58	0.09 ± 0.00	-	1,115 ± 56	175 ± 9
KRG16-06	3.60 ± 0.13	-	1.66 ± 0.06	15.95 ± 0.64	0.11 ± 0.00	-	267 ± 50	74 ± 14
KRG16-101	3.97 ± 0.33	-	1.90 ± 0.08	18.27 ± 0.93	0.10 ± 0.01	-	141 ± 11	36 ± 3
KRG16-104	4.42 ± 0.23	-	1.62 ± 0.13	14.60 ± 1.49	0.10 ± 0.01	-	307 ± 18	69 ± 4
KRG16-111	4.54 ± 0.42	-	1.58 ± 0.08	14.97 ± 0.88	0.10 ± 0.01	-	-	168 ± 251*

*Ages calculated from single aliquot additive dose response curve.

Table 2: Summary of sample luminescence kinetic parameters. Full details of environmental dose rate derivation are given in the Supplementary Material. Ages in italics are saturated. Maximum ages are calculated from $2 * D_0$.

Sample	Signal	\dot{D} (Gy ka ⁻¹)	D_0 (Gy)	E_c (eV)	$\log_2(s)$ (s ⁻¹)	E_u (eV)	$\log_2(\rho')$	\bar{n}	\bar{n}_{ss}	Age (ka)	Max. Age (ka)
KRG05	IRSL50	8.57 ± 1.17	848 ± 29	1.33 ± 0.02	9.31 ± 0.21	0.07 ± 0.01	-5.27 ± 0.08	0.25 ± 0.06	0.23 ± 0.07	<i>404.62^{23.17}_{23.75}</i>	184
	IRSL100		817 ± 20	1.38 ± 0.03	9.09 ± 0.24	0.07 ± 0.01	-5.45 ± 0.06	0.36 ± 0.07	0.38 ± 0.05	<i>243.05^{196.60}_{16.42}</i>	182
	IRSL150		837 ± 21	1.32 ± 0.04	8.02 ± 0.34	0.09 ± 0.01	-5.73 ± 0.10	0.55 ± 0.06	0.60 ± 0.08	<i>236.51^{126.66}_{30.10}</i>	191
	IRSL225		701 ± 21	1.34 ± 0.05	7.53 ± 0.43	0.13 ± 0.01	-5.98 ± 0.06	0.65 ± 0.03	0.76 ± 0.03	<i>157.06^{60.03}_{19.67}</i>	162
KRG06	IRSL50	7.10 ± 0.47	829 ± 39	1.36 ± 0.03	9.57 ± 0.25	0.06 ± 0.01	-5.04 ± 0.04	0.06 ± 0.01	0.08 ± 0.02	<i>121.37^{36.00}_{21.99}</i>	206
	IRSL100		1002 ± 39	1.41 ± 0.03	9.41 ± 0.28	0.07 ± 0.01	-5.18 ± 0.05	0.07 ± 0.01	0.16 ± 0.03	<i>67.40^{9.96}_{9.24}</i>	258
	IRSL150		980 ± 36	1.35 ± 0.04	8.28 ± 0.37	0.08 ± 0.01	-5.45 ± 0.05	0.11 ± 0.01	0.38 ± 0.04	<i>44.75^{4.36}_{2.22}</i>	265
	IRSL225		791 ± 32	1.41 ± 0.06	8.12 ± 0.49	0.13 ± 0.01	-5.54 ± 0.04	0.18 ± 0.01	0.46 ± 0.04	<i>52.31^{1.37}_{4.20}</i>	216
KRG101	IRSL50	6.57 ± 1.43	910 ± 46	1.52 ± 0.03	11.06 ± 0.12	0.07 ± 0.00	-5.05 ± 0.04	0.08 ± 0.00	0.09 ± 0.02	<i>217.09^{27.72}_{23.78}</i>	244
	IRSL100		1029 ± 44	1.39 ± 0.03	9.29 ± 0.27	0.08 ± 0.01	-5.33 ± 0.03	0.11 ± 0.00	0.27 ± 0.03	<i>71.51^{3.08}_{3.88}</i>	295
	IRSL150		1105 ± 45	1.40 ± 0.03	8.77 ± 0.25	0.09 ± 0.01	-5.49 ± 0.05	0.13 ± 0.00	0.41 ± 0.04	<i>61.60^{1.92}_{1.90}</i>	324
	IRSL225		892 ± 37	1.29 ± 0.04	7.14 ± 0.36	0.13 ± 0.01	-5.77 ± 0.07	0.20 ± 0.00	0.63 ± 0.05	<i>50.73^{1.37}_{1.36}</i>	267
KRG104	IRSL50	6.20 ± 0.85	784 ± 34	1.33 ± 0.03	9.14 ± 0.20	0.08 ± 0.01	-5.19 ± 0.01	0.09 ± 0.01	0.17 ± 0.01	<i>80.15^{15.72}_{13.84}</i>	231
	IRSL100		709 ± 29	1.37 ± 0.02	8.88 ± 0.21	0.09 ± 0.01	-5.45 ± 0.03	0.16 ± 0.04	0.38 ± 0.02	<i>57.57^{22.00}_{18.31}</i>	219
	IRSL150		777 ± 31	1.41 ± 0.03	8.93 ± 0.27	0.09 ± 0.01	-5.57 ± 0.04	0.18 ± 0.04	0.48 ± 0.04	<i>56.76^{16.97}_{4.88}</i>	243
	IRSL225		709 ± 31	1.39 ± 0.04	8.12 ± 0.34	0.13 ± 0.01	-5.65 ± 0.07	0.24 ± 0.05	0.55 ± 0.05	<i>63.32^{17.81}_{13.35}</i>	223
KRG111	IRSL50	7.03 ± 1.58	615 ± 32	1.38 ± 0.02	9.47 ± 0.19	0.08 ± 0.00	-5.29 ± 0.02	0.00 ± 0.00	0.25 ± 0.02	<i>0.64^{0.06}_{0.06}</i>	164
	IRSL100		871 ± 43	1.38 ± 0.02	8.12 ± 0.33	0.09 ± 0.01	-5.63 ± 0.14	0.00 ± 0.00	0.53 ± 0.11	<i>0.99^{0.04}_{0.04}</i>	241
	IRSL150		932 ± 39	1.40 ± 0.04	7.85 ± 0.56	0.09 ± 0.01	-5.81 ± 0.22	0.01 ± 0.00	0.66 ± 0.16	<i>1.16^{0.18}_{0.18}</i>	261
	IRSL225		748 ± 33	1.34 ± 0.05	6.46 ± 0.52	0.12 ± 0.01	-5.86 ± 0.17	0.01 ± 0.00	0.69 ± 0.11	<i>1.39^{0.32}_{0.32}</i>	210
KRG112	IRSL50	7.06 ± 1.54	572 ± 31	1.35 ± 0.02	9.90 ± 0.15	0.07 ± 0.00	-5.32 ± 0.01	0.00 ± 0.00	0.28 ± 0.01	<i>0.29^{0.02}_{0.02}</i>	151
	IRSL100		807 ± 37	1.34 ± 0.02	9.34 ± 0.18	0.08 ± 0.00	-5.62 ± 0.10	0.00 ± 0.00	0.52 ± 0.08	<i>0.32^{0.08}_{0.08}</i>	221
	IRSL150		847 ± 32	1.36 ± 0.03	9.12 ± 0.27	0.10 ± 0.00	-5.92 ± 0.32	0.00 ± 0.00	0.72 ± 0.21	<i>0.36^{0.12}_{0.12}</i>	236
	IRSL225		768 ± 35	1.27 ± 0.04	7.78 ± 0.33	0.12 ± 0.01	-6.04 ± 0.24	0.00 ± 0.00	0.78 ± 0.13	<i>0.44^{0.08}_{0.08}</i>	215

5

10

15

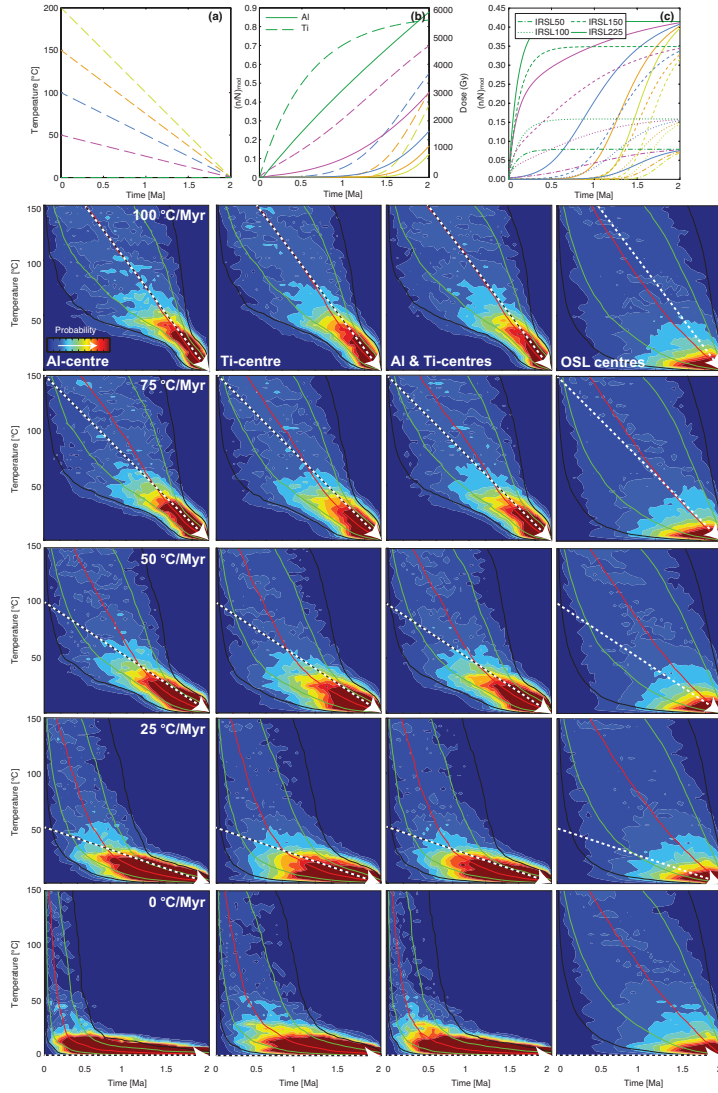
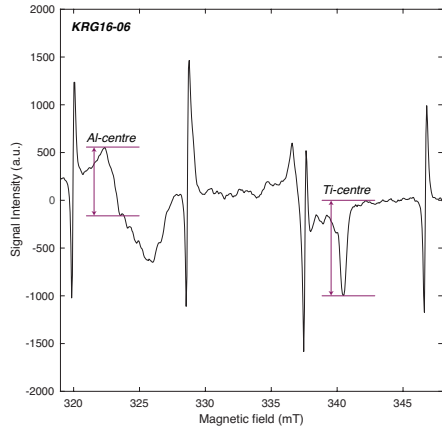


Figure 1: Synthetic inversions of ESR and OSL data for monotonic cooling of 100 °C/Myr, 75 °C/Myr, 50 °C/Myr, 25 °C/Myr and no cooling. (a) Cooling histories and (b) forward modelled Ti (primary y-axis) and Al (secondary y-axis) centre signal accumulation, (c) OSL centre signal accumulation. ESR and OSL signals after 2 Myr were then inverted to derive cooling histories for the Al and Ti and OSL centres, as well as for the Al and Ti-centres combined for the different cooling scenarios. The original cooling history from (a) is shown as a white dashed arrow in each of the cooling histories, whilst the 1 and 2 σ and median cooling histories are shown in green, black and red respectively.



Formatted: Centered

Fig 2: Natural ESR spectrum of sample KRG16-06. The spectrum of the internal MgO:Mn standard overprints the quartz ESR spectrum, but does not affect the Al and Ti centre integration ranges used (indicated on the figure).

Formatted: Caption

Formatted: English (US)

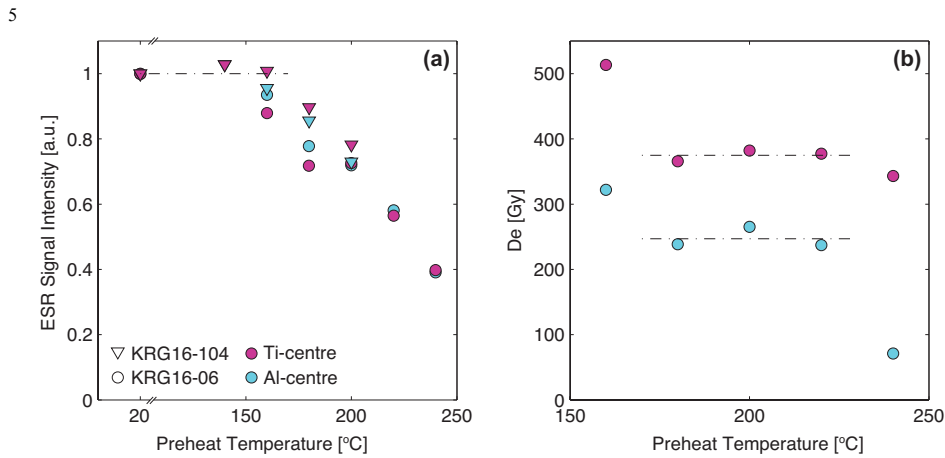
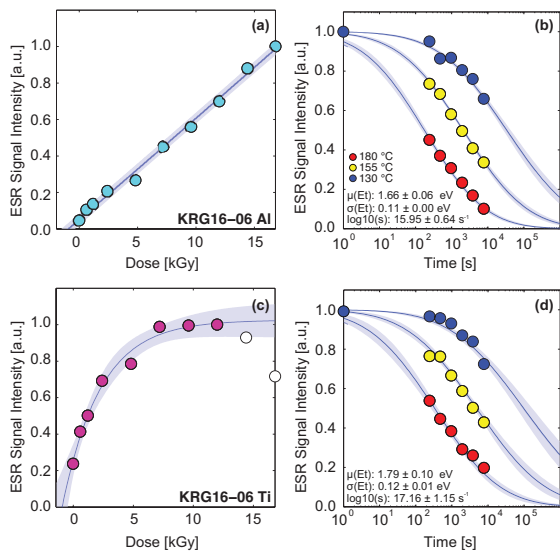


Figure 23: (a) Changing ESR signal intensity with increasing preheat temperature for KRG16-06 (two minute preheats) and KRG16-104 (four minute preheats). Signal intensities are normalised relative to measurements made following no preheating (shown at 20 °C). (b) Preheat plateau data for KRG16-06 based on measurement of a single aliquot at each temperature (two minute preheats).



5 **Figure 34:** ESR dose response and isothermal decay for the Al (a,b) and Ti-centres (c,d) of sample KRG16-06. Whereas the Al-centre (a) experiences linear signal accumulation, the Ti-centre (b) follows exponential growth before the signal intensity starts to reduce (white data points). This reduction in signal intensity is thought to represent radiation dose quenching of the ESR signal (cf. Woda and Wagner, 2007; Tissoux et al., 2007; Duval and Guilarte, 2015) and these data were excluded before fitting. The isothermal decay of the Al (a) and Ti-centres (b) is fitted with a density of states model assuming a Gaussian distribution around trap depth (Lambert et al., In Review).

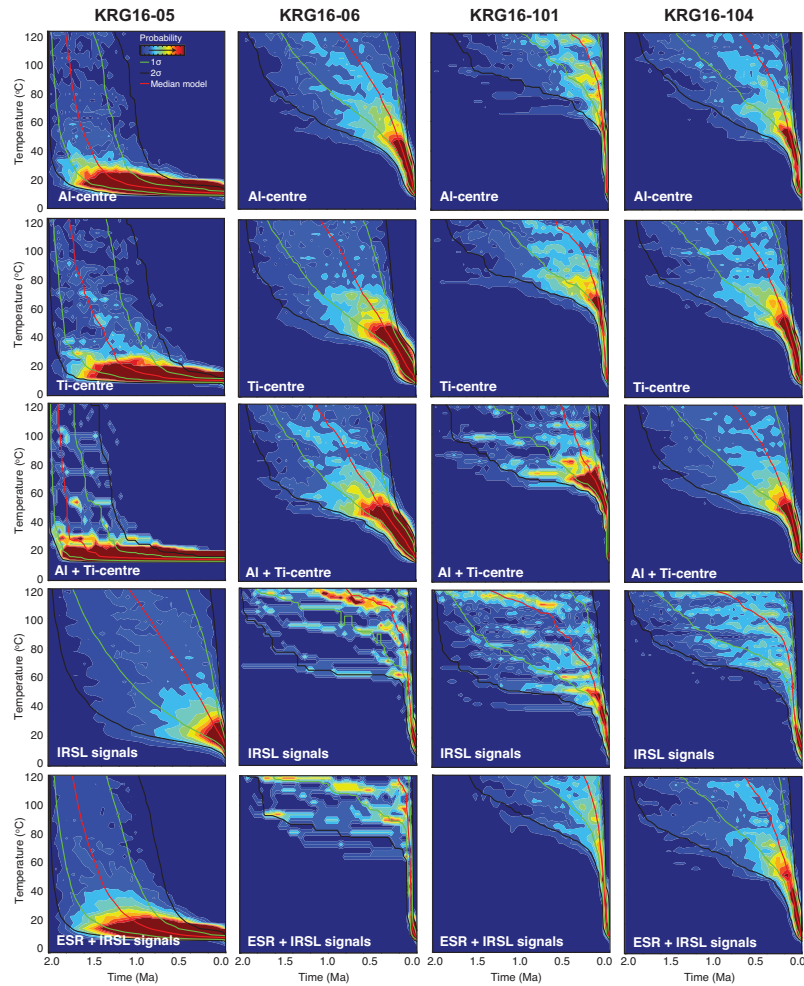


Figure 45: Probability density functions of cooling histories inverted from the ESR and OSL data of samples KRG16-05, KRG16-06, KRG16-101 and KRG16-104. The different rows show inversion of the Al-centre, the Ti-centre, the Al and Ti-centres together, all four OSL signals (i.e. IRSL₅₀, IRSL₁₀₀, IRSL₁₅₀, IRSL₂₂₅) and finally the Al and Ti-centres, and the OSL centres together. Time-temperature histories were generated over 2 Myr with random monotonic cooling from 200 °C to 15 ± 5 °C. All probability density functions are scaled relative to 1. Model residuals for the inversion of all signals together are shown in the Supplementary Material.

5

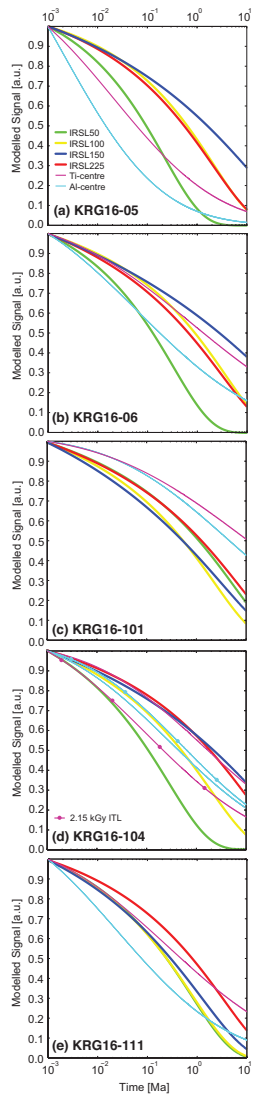


Figure 56: Thermal stability of ESR signals in comparison to IRSL signals. The isothermal decay of (a) KRG16-05, (b) KRG16-06, (c) KRG16-101, (d) KRG16-104 and (e) KRG16-111 were modelled using the kinetic parameters listed in Tables 1 and 2 under isothermal conditions of 20 °C. Anomalous fading signal loss has been included in modelling of the IRSL data.

